Research Square

Preprints are preliminary reports that have not undergone peer review.
They should not be considered conclusive, used to inform clinical practice,
or referenced by the media as validated information.

Optimized Serpentine Dean-Flow UV-C Processing Provides Microbial Safety and Better Preserves Bioactive Components in Donor Human Milk Than Holder Pasteurization

Md Abdul Wazed
Oregon State University
Jestin Bose
Tennessee State University
Nirmal Thirunavookarasu
Tennessee State University
Hussein Mohamed
Oregon State University
Bishal Barman
Oregon State University
Richard L. Lumata
Oregon State University
Brahmaiah Pendyala
Tennessee State University
Ankit Patras
Tennessee State University
Joy Waite-Cusic
Oregon State University
David C. Dallas
dave.dallas@oregonstate.edu
Oregon State University

Article

Keywords: Non-thermal pasteurization, breast milk, mother's milk, irradiation, preterm infant health, functional proteins

Posted Date: November 24th, 2026

DOI: https://doi.org/10.21203/rs.3.rs-11544159/v1

License: This work is licensed under a Creative Commons Attribution 4.0 International License.
Read Full License

Additional Declarations: No competing interests reported.

Research Article

Optimized Serpentine Dean-Flow UV-C Processing Provides Microbial Safety and Better Preserves Bioactive Components in Donor Human Milk Than Holder Pasteurization

Authors:

Md Abdul Wazed[1], Jestin Bose[2], Nirmal Thirunavookarasu[2], Hussein Mohamed[3], Bishal Barman[3], Richard L. Lumata[1], Brahmaiah Pendyala[2], Ankit Patras[2], Joy Waite-Cusic[3], David C. Dallas[1,3*]

[1]Nutrition Program, School of Nutrition and Public Health, College of Health, Oregon State University, Corvallis, OR 97331, USA

[2]Department of Food and Animal Sciences, Tennessee State University, Nashville, TN 37209, USA

[3]Department of Food Science and Technology, Oregon State University, Corvallis, OR 97331, USA

*Correspondence: dave.dallas@oregonstate.edu (D.C.D)

Abstract:

Conventional Holder pasteurization (HoP; 62.5 °C for 30 min) for processing donor human milk (DHM) in milk banks provides microbial safety but significantly reduces bioactive components that support infant health. As an alternative to HoP, we examined UV-C treatment using a serpentine Dean-flow system applied at <10 °C. Optical properties of pooled DHM were determined. Computational fluid dynamics (CFD) was performed to determine the velocity magnitude and incident radiation fields in the reactor. The efficacy of the UV-C system against *Enterococcus faecium* (ATCC 8459) and *Salmonella* Muenchen (ATCC BAA-1674) was evaluated at 2–29.4 mJ/cm^2 doses. Milk samples exposed to each UV-C treatment dose and HoP were examined for preservation of lactoferrin, IgA, bile salt-stimulated lipase, lysozyme, vitamin A and vitamin E compared with raw milk. A UV-C dose of 28 mJ/cm^2 provided >5-log reductions for both microorganisms tested, achieving microbial safety comparable to HoP. UV-C treatment at this dose preserved significantly more lactoferrin (88.3%), IgA (89%), bile salt-stimulated lipase (BSSL) activity (74.4%) and lysozyme activity (72%) than HoP ($p < 0.05$). UV-C treatment preserved significantly more Vitamin A than HoP, while both the treatments retained similar levels of vitamin E (α-tocopherol). Neither UV-C nor HoP significantly increased lipid oxidation products (malonaldehyde). This study demonstrates the potential of a serpentine Dean-flow UV-C system as an effective alternative pasteurization method that preserves bioactive components that can impact the health of vulnerable preterm infants.

Keywords: Non-thermal pasteurization; breast milk; mother's milk; irradiation; preterm infant health; functional proteins.

1. Introduction

Approximately 10% of infants are born preterm (<37 weeks of gestation) and experience less in utero development than term infants, rendering them vulnerable to poor growth, increased risk for gastrointestinal diseases, infections and poor neurological development (Collins, Weitkamp, & Wynn, 2018; Tanner et al., 2015). Part of the poor growth outcomes observed in preterm infants is likely due to their limited nutrient digestive and absorptive function compared with term infants (Demers-Mathieu et al., 2018). Human milk is recognized as the optimal nutrition source for preterm infants (albeit with fortification). It provides essential nutrients and bioactive factors that help protect against infections, enhance immune development and support optimal growth (Ballard & Morrow, 2013; Conboy-Stephenson et al., 2024). Donor human milk (DHM) is often provided to preterm infants when parent's own milk is insufficient or unavailable, as it improves outcomes compared with infant formula (Quigley, Embleton, & McGuire, 2019). To enhance microbial safety, milk banks treat DHM via Holder pasteurization (HoP) (heating milk at 62.5 °C for 30 min) (Moro et al., 2019; Peila et al., 2017). Though effective in achieving microbial safety (>5-log reductions in vegetative bacteria), HoP substantially degrades bioactive proteins and enzymes such as lactoferrin, lysozyme, immunoglobulin A (IgA) and bile salt-stimulated lipase (BSSL) (Koh et al., 2020; Liang et al., 2024). Lactoferrin has potent antibacterial, antiviral and immunomodulatory functions and supports iron absorption (Cao et al., 2023). IgA assists in enhancing gut mucosal immunity, protecting against enteric pathogens (Walker, 2010). Lysozyme disrupts bacterial cell walls, providing broad-spectrum antibacterial activity (Ferraboschi, Ciceri, & Grisenti, 2021). BSSL facilitates digestion of human milk lipids (Bertino et al., 2013; He et al., 2020). Unfortunately, the bioactive degradation from HoP may limit the health benefits for preterm infants provided by human milk (Peila et al., 2017). Therefore, there is a need for non-thermal pasteurization alternatives that can provide microbial safety for DHM without compromising bioactive components. UV-C irradiation has been shown to have effective bactericidal properties and minimal impact (depending on dose applied) on bioactive components and their functionalities (Barman et al., 2026; Kim, Ryan, & Dallas, 2025; Koutchma, 2018; Liang et al., 2024; Patras et al., 2021). However, applying UV-C technology to human milk is challenging. Human milk is opaque and viscous, containing significant amounts of fat, proteins and bioactive molecules that strongly absorb UV-C radiation, thus limiting penetration depth and creating uneven dose

distribution in static systems (Gunter-Ward et al., 2018). Some UV-C reactors would not provide uniform dose delivery in opaque milk, necessitating high irradiation doses, which may lead to nutritional degradation and undesirable oxidation reactions (Matak et al., 2005).

To achieve uniform dose delivery, reactors designed to enhance fluid mixing and UV-C fluence distribution, such as serpentine Dean-flow systems have been developed (Patras et al., 2021; Pendyala et al., 2021). The serpentine Dean-flow UV-C system is designed with a coiled tube geometry to induce secondary flow vortices, known as Dean vortices, to enhance radial mixing and enhance the uniformity of UV-C exposure to all milk particles (Vashisht et al., 2022). Previous studies employing serpentine Dean-flow reactors for whole bovine and almond milk demonstrated effective microbial inactivation (>5-log reduction of vegetative pathogens) with minimal oxidative changes compared with traditional thermal treatments (Pendyala et al., 2022; Vashisht et al., 2022). However, no study has yet examined the dose of UV-C provided by serpentine UV-C treatment required for >5-log reduction of vegetative pathogens or its effects on bioactive proteins in DHM.

Therefore, this study evaluates the effectiveness of a serpentine Dean-flow UV-C system for microbial safety and intact bioactive preservation in DHM compared with HoP. We investigated the efficacy of this system against relatively UV-C-resistant gram-positive *Enterococcus faecium* (ATCC 8459) and gram-negative *Salmonella enterica* serovar Muenchen (ATCC BAA 1674). Additionally, we assessed preservation of critical bioactive proteins (lactoferrin and IgA), enzymatic activities (BSSL and lysozyme), vitamins (A and E) and the extent of lipid oxidation by measuring the malondialdehyde (MDA) content.

2. Materials and Methods

2.1 DHM sample collection

To examine the effect of processing on microbial reduction and preservation of an array of bioactive components, frozen, raw human milk (>40 L) was collected from Northwest Mothers Milk Bank (NWMMB, Portland, OR, USA), which managed the informed consent procedure. Bags of frozen DHM from individual donors were kept in a 4 °C refrigerator for 48 h to thaw. DHM from milk bags were mixed after thawing to prepare 3 different pools, aliquoted into polypropylene containers (300 mL each) and stored immediately at –20 °C until further analysis. The nutritional composition of three pooled DHM was determined via LactoScope

FTIR (Perten Instruments, Hägersten, Sweden) (Supplementary Table 1). The frozen DHM samples (300 mL/container) were shipped on dry ice to Tennessee State University, TN, USA for optical analysis, numerical simulation of fluid velocity magnitude and incident radiation using computational fluid dynamics (CFD), bacterial inoculation, bacterial D-value calculation and serpentine Dean-flow UV-C treatments. Treated samples were shipped on dry ice to Oregon State University, OR, USA for further analysis. The samples underwent two freeze-thaw cycles before analysis.

2.2. Measurement of optical properties of DHM

In order to calculate UV-C dose delivered to milk during our collimated beam experiments (see next section) and at specific times of exposure (passes) within the serpentine Dean flow UV-C system, DHM optical properties, including total transmittance and diffuse reflectance (8° geometry), were measured for each pool of milk using a double-beam spectrophotometer (Cary 100, Agilent Technologies, USA) equipped with a 6-inch integrating sphere (Lab sphere DRA-CA-30, Agilent Technologies, USA) at the 254 nm wavelength as previously described (Gunter-Ward et al., 2018). Measurements were performed using thin synthetic quartz cuvettes that are optically identical across samples and thin enough to ensure measurable signals in the highly absorbing milk matrix (0.08 and 0.1 mm path length). Each DHM sample was analyzed in triplicate, with instrument baseline and reference corrections. Because light transmission in opaque scattering fluids is governed by the Radiative Transfer Equation (RTE), we determined the absorption coefficient (μ_a) and reduced scattering coefficient (μ'_s) from the integrating-sphere measurements. The inverse adding doubling (IAD) program was used to estimate μ_a and μ'_s by applying total transmittance, reflectance and the refractive index as input values (Prahl, 1999). The resulting μ_a and μ'_s values were used to calculate UV-C fluence rate and fluence for the collimated beam experiments and for specific exposure times in the continuous-flow UV-C system (Patras et al., 2021; Singh et al., 2025; Vashisht et al., 2021). From the obtained optical properties, ultraviolet transmittance (UVT, %/cm), which indicates the fraction of the incident light transmitted through a fluid over a 1 cm path length, was calculated as per equation (1).

$$\text{UVT } (\%/cm) = [10^{-A}] \times 100 \qquad (1)$$

Where A is the absorbance coefficient (base 10) of the DHM sample at 254 nm that corresponds to a 1 cm path length.

2.3. Numerical simulation of fluid velocity magnitude and incident radiation

The velocity magnitude and incident UV-C irradiation within the serpentine Dean-flow system during DHM processing were predicted numerically using ANSYS Fluent 2025 R1 (ANSYS Inc., Canonsburg, PA, USA), following our previously published method (Singh et al., 2025). A three-dimensional model of a representative section of the FEP tube path (2.38 mm internal diameter), including consecutive sharp bends with a 2 cm bend radius, was constructed in ANSYS SpaceClaim. The fluid domain was discretized into more than 900,000 tetrahedral elements using ANSYS Meshing. DHM was treated as an incompressible Newtonian fluid (ρ = 1,035 kg·m^{-3}; $\mu = 2.2 \times 10^{-3}$ Pa·s). Because the Reynolds number at the operating flow rate (Re = 2,012) was below the laminar–turbulent transition threshold (Re ≈ 2,300), the continuity (equation 2) and Navier–Stokes (equation 3) equations were solved for steady, incompressible laminar flow:

$$\nabla \cdot \vec{V} = 0 \qquad (2)$$

$$\rho\left(\vec{V} \cdot \nabla\right)\vec{V} = -\nabla P + \mu \nabla^2 \vec{V} \qquad (3)$$

Where ρ is the fluid density (kg/m^3), μ is the dynamic viscosity (Pa·s), V is the velocity vector (m/s) and P is the pressure (Pa). A uniform inlet velocity of 1.80 m/s was specified, corresponding to a calibrated flow rate of 480 mL/min. A pressure outlet and no-slip walls were also specified. Pressure–velocity coupling used the SIMPLE algorithm with second-order upwind discretization of the momentum equations. Convergence was reached when all residuals fell below 1×10^{-5}.

UV-C irradiation at 254 nm was simulated using the Discrete Ordinates (DO) radiation model with 8 × 8 angular discretization and 6 × 6 pixelation, and the lamp wall was set as the irradiation source boundary. The DO model solves the radiative transfer equation (RTE) over discrete solid angles (equation 4):

$$\frac{dI(r,s)}{ds} + (a + \sigma_s) I(r,s) = \frac{\sigma_s}{4\pi} \int_{4\pi} I\,(r,s') \Phi(s \cdot s')\, d\Omega' \qquad (4)$$

where I is the radiation intensity (W·m^{-2}·sr^{-1}), r is the position vector, s and s′ are the propagation and scattering direction vectors, a is the absorption coefficient (m^{-1}), σ_s is the scattering coefficient (m^{-1}), Φ is the scattering phase function, and Ω' is the solid angle. Clear juices can be modeled as absorption-only, but DHM scatters UV-C because of its colloidal fat globules and casein micelles. Although scattering in DHM is minor relative to absorption

(Section 3.1), fat globules and casein micelles contribute some scattering; the scattering term was therefore retained, using the measured absorption coefficient (21.13 cm^{-1}), scattering coefficient (1.92 cm^{-1}) and refractive index (1.39) (Section 2.2). Velocity contours were extracted at cross-sections of 0°, 45°, 90°, 135° and 180° along a bend, together with three-dimensional streamlines and the cross-sectional irradiation distribution.

2.4. Microbial strains and culture conditions

To evaluate the pathogen-inactivation potential of a serpentine Dean-flow UV-C system in DHM, representative gram-positive *E. faecium* (ATCC 8459) and gram-negative *S.* Muenchen (ATCC BAA 1674) strains were cultured. Both strains were procured from the American Type Culture Collection (ATCC) center (Manassas, VA, USA). Both microbial cultures were propagated using Tryptic Soy Broth (Oxoid Ltd., Basingstoke, UK) in a shaker incubator at 37 °C to provide aeration. After successive propagation, the microbial cultures were harvested by centrifuging at 1,677 × *g* for 4 min (Pendyala et al., 2020). The supernatant was discarded, and the resulting pellet was dissolved in phosphate-buffered saline (PBS, Becton Dickinson, NJ, USA) to remove impurities. The microbial cells were washed twice and resuspended in PBS to a final volume of 30 mL, yielding a cell concentration of 10^9 CFU/mL. This microbial solution was mixed with the prepared pools of DHM samples (2 L) and used for microbial inactivation experiments using a serpentine Dean-flow UV-C system (Akwu et al., 2023; Singh et al., 2025).

2.5. UV-C Sensitivity of test organisms

The D_{10} value (dose required for 90% inactivation) of *S.* Muenchen (ATCC BAA 1674) was previously reported as 4.1 mJ/cm^2 (Pendyala et al., 2020). However, the D_{10} value of *E. faecium* (ATCC 8459) was evaluated in this study using a Collimated Beam System (Trojan Technologies, Canada) equipped with a 25 W low-pressure mercury lamp. The microorganism was cultured and propagated as mentioned in section 2.4. After two successive propagations, the cultures were harvested and resuspended in PBS to a concentration of approximately 10^7 to 10^8 CFU/mL. The test solution absorbance was measured using a double-beam spectrophotometer (Cary 100, Agilent Technologies, USA) equipped with a 6-inch integrating sphere (Lab sphere DRA-CA-30, Agilent Technologies, USA) at 254 nm wavelength. Then, known UV doses were delivered to 5 mL of the microbial solution, accounting for all loss factors using the standard dose-estimation protocol described previously (Bolton & Linden, 2003). The microbial test

solution was continuously stirred with a magnetic stirrer to ensure uniform dose distribution and mixing throughout the experiment. The D_{10} value was evaluated using the Weibull model fitted using the GInaFiT Excel add-in. All the treatments were done in triplicate.

2.6. UV-C treatment of DHM

Human milk samples were subjected to UV-C treatment using a continuous serpentine Dean-flow system. For this system, a fluorinated ethylene propylene tube (FEP) of 6.7 m with a transmittance of 60% and an internal diameter of 2.38 mm was wound in a serpentine path using the holes provided in the metal casing of the system in which 4 m of the tube was exposed to direct UV-C irradiation. The serpentine tube had bends with a bend radius of 2 cm, which changed the fluid path and created Dean vortices at these sharp bends. The UV-C system also includes a cooling fan to remove the heat generated during its operation. The system consists of a 40 W (12 W output) low-pressure mercury vapor lamp, which emits UV-C irradiation at 253.7 nm, placed at the center of the system. The system also includes a built-in UV-C ballast and a 4–16 mA circuit that monitors the power drawn by the lamp. We adjusted the fluid flow rate using a peristaltic pump (Watson-Marlow, USA) and performed a bucket test to determine the exact flow rate during each treatment (Singh et al., 2025).

While using the Dean-flow UV-C system, we first calculated the Reynolds number and then the Dean number to determine the flow properties of DHM using the following equations:

$$R_e = \frac{\rho V D}{\mu} \qquad (5)$$

where ρ denotes the density of the raw DHM (kg/m^3), V indicates the flow velocity (m/s), D is the internal flow-tube diameter (m) and μ is the dynamic viscosity of the fluid (Pa·s) measured with a rheometer (TA Instruments, Model AR G2, West Sussex, UK).

The centrifugal forces generated at the bends of the flow path induce secondary (Dean) flow that enhances radial mixing within the fluid, resulting in a uniform radial UV fluence distribution. The Dean number was determined using equation 6.

$$De = Re\sqrt{\frac{D}{D_c}} \qquad (6)$$

The Dean number is a function of the Reynolds Number (Re), the hydraulic diameter of the tube (D) and the diameter of the coil (Dc). The system maintained an average flow rate of 480 mL/min for UV-C treatment of three DHM pools. To avoid contamination, cleaning-in-place

(CIP) procedures were conducted by circulating the CIP solution (Vesphene II, Steris Corporation, USA) through the system loop for 3 min using a peristaltic pump, followed by flushing with 1 L of deionized water. A CIP was performed both before and after each experimental run.

The UV-C treatment of DHM samples was performed under chilled conditions (<10 °C), with an inlet temperature of 4 °C and an outlet temperature of 8.7 °C. DHM was exposed to UV-C fluence at 480 mL/min across sequential passes through the UV-C system. All experiments were performed in triplicate. A 10 mL sample was collected after each pass into sterile 15 mL centrifuge Falcon tubes. After UV-C treatment, samples were immediately placed in an ice bath to cool rapidly, then frozen at –20 °C for shipping on dry ice for further analysis at Oregon State University. For travel controls for microbial inactivation and bioactive preservation studies, both inoculated and uninoculated samples were shipped with the other samples and exposed to the same freezing and thawing conditions as the test samples. All samples were frozen and thawed twice before analysis throughout sample preparation and experimentation. The reduction equivalent fluence (REF) delivered during UV-C treatment was calculated using the biodosimetry approach as described previously (Pendyala et al., 2020). Briefly, the log reduction of *S.* Muenchen (ATCC BAA 1674) after UV-C exposure and the D_{10} value were used to back-calculate the corresponding REF delivered using equation 7.

$$\text{Reduction equivalent fluence (REF)} = \text{Log reduction} \times D_{10} \qquad (7)$$

2.7. Holder Pasteurization of DHM

To compare the effects of UV-C processing and conventional HoP on the preservation of bioactive components, we treated 3 pools of DHM samples by HoP. HoP was performed in a pre-heated water bath (set at 62.5 °C) using a Falcon tube with 25 mL uninoculated DHM. The tube was held in the water bath for 30 min after reaching the target temperature of 62.5 °C to mimic the HoP treatment followed by non-profit human milk banks. After HoP, samples were immediately placed in an ice bath for rapid cooling, then frozen at –20 °C until further analysis.

2.8. Enumeration of microbial counts

Microbial analysis was conducted on DHM samples inoculated with *E. faecium* (ATCC 8459) or *S.* Muenchen (ATCC BAA 1674) before and after UV-C treatment to determine the effect of processing on microbial safety. Microbial counts were determined using the standard

10-fold serial dilution method in 0.1% sterile peptone water. From each dilution, 100 µL was spread onto Tryptic Soy Agar (TSA; Neogen, USA) for *E. faecium* (ATCC 8459) and Hektoen Enteric (HE) agar (Neogen, USA) for *S.* Muenchen (ATCC BAA 1674). Plates were incubated aerobically at 37 °C for 48 h. Enumerated colonies were expressed as log colony-forming units per milliliter (log CFU/mL). Log reductions were calculated by comparing microbial counts of UV-C-treated samples with their corresponding controls.

2.9. Quantification of bioactive proteins by ELISA

The preservation of lactoferrin and IgA was measured in untreated (travel control), UV-C-treated and HoP-treated DHM samples to determine the effect of processing on bioactive components. Concentrations of lactoferrin and IgA were determined using a human lactoferrin ELISA kit (Invitrogen, catalog # EH309RB) and an IgA human ELISA kit (Invitrogen, catalog # BMS2096), respectively, following the manufacturer's protocol.

2.10. Quantification of enzyme activity

The enzymatic activity of DHM was examined in untreated (travel control), UV-C-treated and HoP-treated DHM samples. Lysozyme activity was measured using a lysozyme activity assay kit (Abcam, catalog # ab211113) following the manufacturer's protocol. To measure BSSL activity in DHM samples, we quantified the concentration of p-nitrophenol cleaved from p-nitrophenyl myristate by BSSL in DHM samples, following our published method (Koh et al., 2020).

2.11. Analysis of vitamin A and E

Vitamins A (retinol) and E (α-tocopherol) were quantified in HoP and UV-C-treated samples to examine the comparative effect of processing on vitamin preservation. UV-C doses that provided >5-log reductions for the tested vegetative bacteria were used because they met the safety threshold. The concentrations of vitamins were measured from the proportional peak areas generated by liquid chromatographs (LCs) and compared with a peak of standard sample. Vitamin A was measured by LC-mass spectrometry (LC-MS) with a Waters TQD mass spectrometer using multiple reaction monitoring data as described previously (Kamao et al., 2007). Vitamin E (α-tocopherol) was quantified by high-performance LC (HPLC) with an amperometric electrochemical detector (ECD) following a published method (Kaushik et al., 2001).

2.12. Total malondialdehyde (MDA) determination via TBARS assay

Total malondialdehyde (MDA) was determined by colorimetric assay using the thiobarbituric acid reactive substances (TBARS) assay, adapted from a published method with modifications (Fenaille et al., 2001). Both treated and untreated DHM (20 µL) were mixed with 150 µL of 0.20 M NaOH, then heated to 60 °C for 30 min to remove bound MDA. The samples were cooled to room temperature and mixed with 400 µL of 1% TBA, 5% TCA, 0.8% butylated hydroxytoluene (BHT) in ethanol. The mixture was vortexed and then centrifuged at 3,000 × *g* for 10 min. A 300 µL aliquot was taken from each sample and transferred into a 1.5 mL microcentrifuge tube for derivatization (70 °C for 1 h). After derivatization, 200 µL aliquots were taken from each sample and transferred into a 96-well plate. Absorbance of the samples at 532 nm was measured in a Spectramax M2 microplate reader using Softmax Pro 7 software. Total MDA was calculated from a standard curve derived from the known concentration of standards, tetramethoxypropane (TMP) derivatized with TBA.

2.13. Data analysis

Optical properties of DHM samples were measured in triplicate and presented as mean ± SD. All microbial inactivation results were converted to a $\log_{10}$ scale for analysis. Reductions were calculated by subtracting each post-treatment microbial count from the raw spiked sample (travel control). We calculated the average log reduction for each microorganism across the 3 DHM pools and 95% confidence interval (CI) at each treatment dose. We considered a dose sufficient when the lower bound of the 95% CI is ≥5 for bacterial inactivation. One-way analysis of variance (ANOVA) followed by Tukey's post-hoc tests was conducted to evaluate significant differences in percentage preservation (compared with raw) for each bioactive protein, enzymatic activity, vitamin and MDA content after UV-C treatments and HoP. Results are presented as mean ± SD and were considered significant at $p < 0.05$.

3. Results and Discussion

3.1. Optical and physical properties of DHM

The observed optical and physical properties of DHM were estimated and reported in Table 1. DHM's absorption coefficient was 21.13 ± 0.35 cm^{-1} and the scattering coefficient was 1.92 ± 0.71 cm^{-1} (Table 1). The refractive index of DHM was 1.39. The UV transmittance of DHM was 1.479 × 10^{-19} %/cm (Table 1). The viscosity and density of DHM were 0.0022 Ns/m^2

and 1,035 kg/m³, respectively (Table 1). The pH of DHM was 6.69 ± 0.01, which indicates that the DHM was of normal quality after shipping and handling.

Table 1: Optical and physical properties of DHM sample

Optical & physical properties	DHM sample
Absorption coefficient (cm^{-1})	21.13 ± 0.35
Scattering coefficient (cm^{-1})	1.92 ± 0.71
Refractive index (at 254 nm)	1.39
Transmittance (%/cm)	1.479×10^{-19}
Density (kg/m^3)	1,035
Viscosity (Ns/m^2)	0.0022
pH	6.69 ± 0.01

The high absorption coefficient (21.13 ± 0.35 cm^{-1}) of DHM is similar to that for bovine whole milk (23.7–24.4 cm^{-1}) reported previously (Pendyala et al., 2022; Vashisht et al., 2022). The measured absorption coefficient indicates that DHM strongly absorbs UV-C irradiation. This finding aligns with previous work showing that milk-based matrices strongly attenuate UV-C irradiation (Gunter-Ward et al., 2018; Pendyala et al., 2022; Vashisht et al., 2022). The high absorption in opaque fluid results in rapid decays of incident UV-C intensity with distance from the irradiated surface which results in steep radial fluence gradients within the matrix (Gunter-Ward et al., 2018; Pendyala et al., 2022; Vashisht et al., 2022). The serpentine Dean-flow UV-C system addresses this radial fluence gradient via strong cross-sectional mixing (Dean vortices) so that fluid elements are repeatedly exposed through higher-fluence zones near the irradiated boundary to receive a uniform cumulative dose (Müller et al., 2011; Pendyala et al., 2022; Vashisht et al., 2022). The scattering coefficient of DHM (1.92 ± 0.71 cm^{-1}) is lower than that of bovine whole milk (>40 cm^{-1}) (Pendyala et al., 2022; Vashisht et al., 2022). This low scattering coefficient of DHM indicates that DHM optical profile is absorption-dominant with a minimal scattering contribution. The refractive index of DHM (1.39) closely aligns with values reported for bovine whole milk (1.4016) (Pendyala et al., 2022; Vashisht et al., 2022). This similarity indicates comparable refraction behavior at the fluid-tube interface across these opaque liquid matrices. The close alignment of refractive indices across DHM and bovine whole milk suggests

that interface-related optical losses are comparable across these matrices. The low UV transmittance of DHM (1.479×10^{-19} %/cm) suggests that only an infinitesimal fraction of incident UV photons can traverse a 1-cm path length, indicating the effective UV-C penetration depth is limited to fractions of a millimeter. From a hydrodynamic perspective, as shown in Table 1, DHM viscosity (0.0022 Ns/m²) and density (1,035 kg/m³) were similar to those of whole bovine milk (0.0019 Ns/m² and 1,029 kg/m³, respectively) reported previously (Vashisht et al., 2022).

3.2. CFD simulation results

3.2.1. Velocity field distribution in the Dean-flow reactor

The velocity magnitude contours of DHM flow through the UV-C reactor were predicted at sequential cross-sectional positions of 0°, 45°, 90°, 135° and 180° along the serpentine tubing path, and are shown in Figure 1a–e. The three-dimensional streamline visualization is presented in Figure 1f. At the reference cross-section (0°, Figure 1a), the velocity profile is asymmetric, with elevated velocity on one side of the tube cross-section, reflecting the influence of the upstream bend on the developing flow field. The maximum velocity predicted by CFD was 2.40 m/s against a calculated average inlet velocity of 1.80 m/s, yielding a V_{max}/V_{avg} ratio of 1.33. In fully developed Hagen–Poiseuille laminar flow, this ratio approaches 2.0; the considerably lower value observed here demonstrates the enhanced radial mixing induced by the Dean vortex effect at the bends. At 45° (Figure 1b), the emergence of counter-rotating secondary flow vortices (Dean vortices) is clearly visible. The centrifugal forces generated as DHM traverses the 2 cm radius bends cause the maximum velocity locus to shift toward the outer wall of the curvature, while lower-velocity fluid occupies the inner wall and central region. The characteristic swirling pattern couples radially displaced fluid elements, effectively transporting milk molecules from low-UV-intensity central zones to high-UV-intensity near-wall regions. The 90° cross-section (Figure 1c) exhibits a well-developed crescent-shaped high-velocity region along the outer wall, consistent with fully established Dean vortex pairs. The inner core shows a distinct low-velocity zone, confirming the shift of momentum toward the outer wall. This cross-section demonstrates the strongest lateral mixing gradient, which is critical for maximizing UV-C dose delivery to fluid elements that would otherwise remain in the radiation-attenuated central zone. The 135° section (Figure 1d) shows a concentrated high-velocity region that has migrated from the outer

periphery to a more centrally biased position as the bend transitions. The asymmetric distribution reflects the evolving secondary flow structure through the second half of the bend. The 180° contour (Figure 1e) demonstrates a broader, more centrally distributed high-velocity region, indicating redistribution of momentum as the flow approaches the straight connector segment. The alternating sharp bends in the serpentine design ensure that Dean vortices are continuously regenerated in alternating rotational directions, preventing the re-stratification of velocity that would occur in a single-curvature coil.

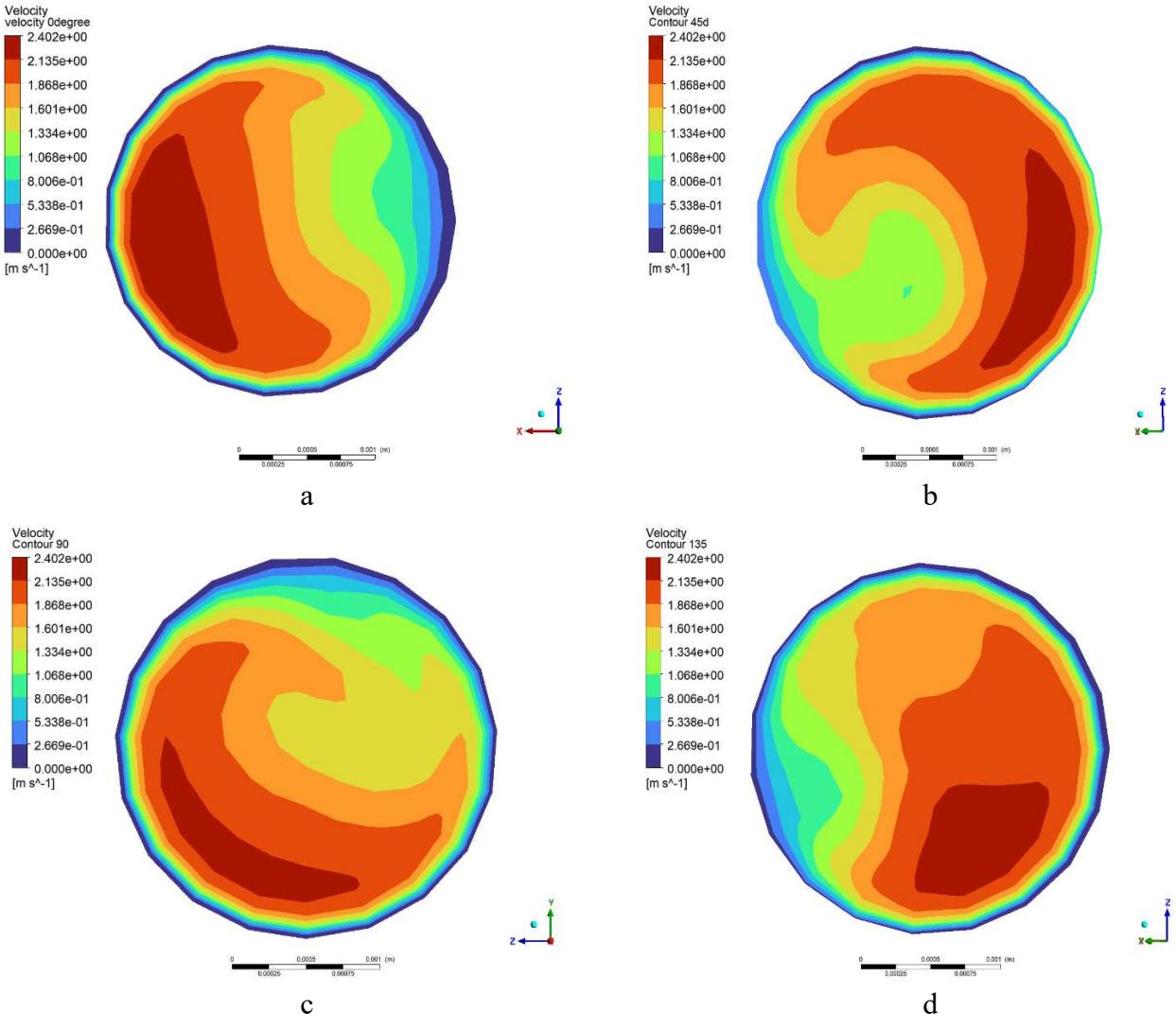

a b

c d

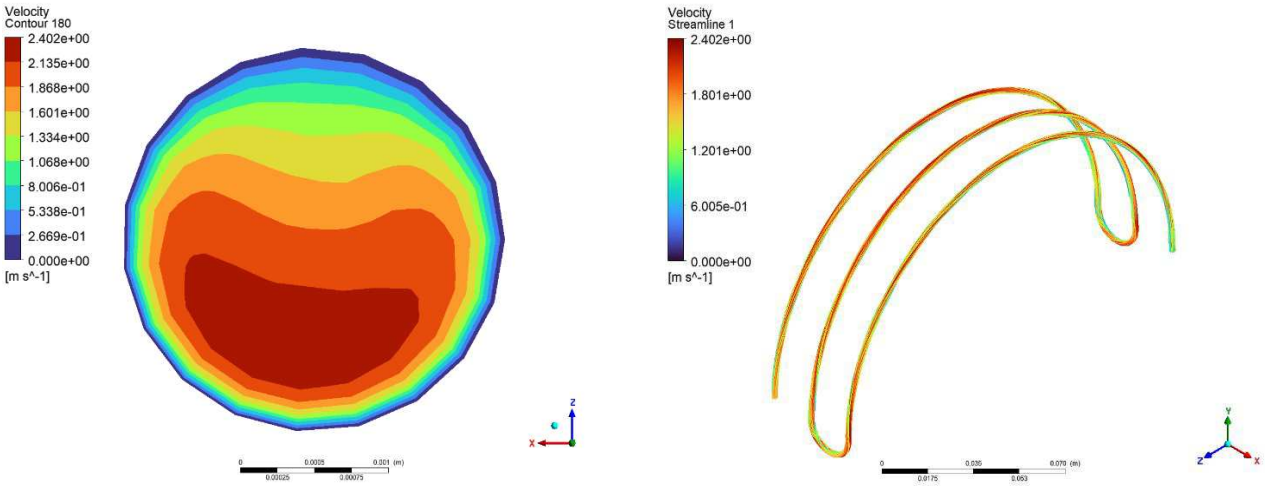

e f

Figure 1. Velocity magnitude contours (m s^{-1}) of DHM in the Dean-flow UV-C reactor at cross-sectional positions: **(a)** 0°, **(b)** 45°, **(c)** 90°, **(d)** 135° and **(e)** 180°. Color scale: 0 (dark blue/black, no-slip wall) to 2.40 m s^{-1} (red). Simulation performed using ANSYS Fluent 2025 R1 with DHM fluid properties (ρ = 1035 kg m^{-3}, $\mu = 2.2 \times 10^{-3}$ Ns/m^2) at a flow rate of 480 mL/min (Re = 2012). **(f)** three-dimensional velocity streamlines of DHM colored by velocity magnitude (m s^{-1}). The helical flow paths demonstrate continuous radial displacement of fluid elements across the tube cross-section throughout the 6.7 m tube length, ensuring exposure of all fluid elements to the near-wall UV-C irradiation zone.

The 3D streamline visualization (Figure 1f) illustrates the helical trajectories of fluid flows through the coiled tube geometry. The streamlines, colored by velocity magnitude, demonstrate that fluid elements travel along distinct helical paths with peak velocities occurring at the outer curvature of each bend (red/orange, ≥2.0 m/s), while slower-moving fluid (green/cyan, ~0.6–1.2 m/s) occupies the inner curvature and transitions between bends. The tightly bundled streamlines confirm organized, laminar helical flow across the full tube length, with no evidence of flow separation or recirculation zones that would create stagnation regions in the reactor.

3.2.2. Discrete Ordinates (DO) irradiation distribution

The UV-C irradiation distribution within the DHM-filled tube cross-section, as predicted by the DO radiation model, is shown in Figure 1g. The irradiation field demonstrates a steep radial gradient, with the maximum irradiation intensity of 19.52 Wm^{-2} occurring at the tube wall

and decreasing sharply toward the tube center, where intensity approaches 0.01 Wm^{-2} (Figure 1g).

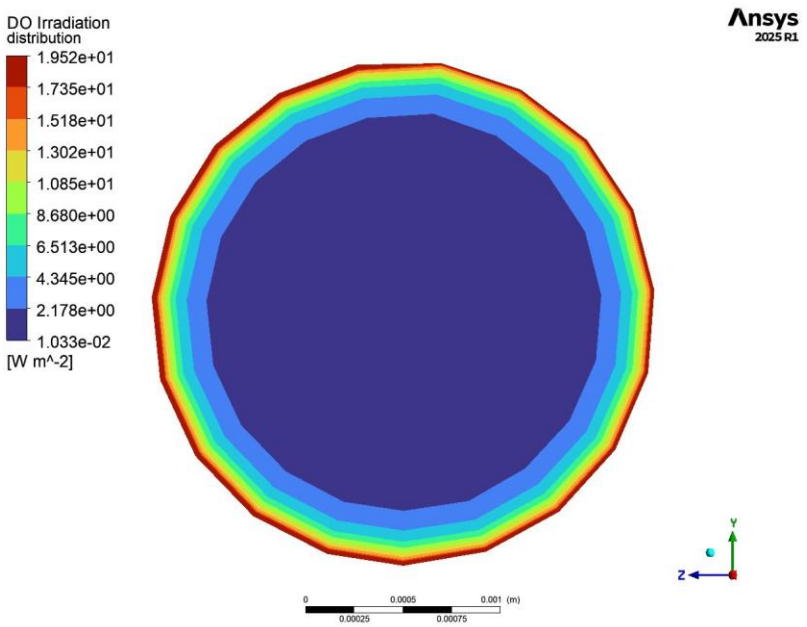

Figure 1g. Discrete Ordinates (DO) irradiation distribution (W m^{-2}) across the DHM-filled tube cross-section as predicted by ANSYS Fluent 2025 R1. Maximum irradiation (19.52 W m^{-2}) occurs at the tube wall; intensity decreases sharply toward the central region due to the high UV-C absorption and scattering properties of DHM (a = 21.13 cm^{-1}, σ_s = 1.92 cm^{-1} at 254 nm).

This pronounced radial attenuation is attributable to the high UV-C absorption coefficient of DHM (a = 21.13 ± 0.35 cm^{-1} at 254 nm), which is among the highest reported for opaque food matrices and is consistent with the near-zero UV transmittance (1.48×10^{-19} %/cm). The steep fluence gradient arises from the combined effects of UV-C photon absorption by DHM chromophores—primarily proteins, lipids, fat globules—and light scattering by colloidal particles. Compared with whole bovine milk (a ≈ 23.7 cm^{-1} (Vashisht et al., 2022)), DHM exhibits intermediate absorption, reflecting its unique protein and lipid composition. The resulting radiation-free dead zone at the tube center indicates the critical importance of efficient radial mixing to ensure all DHM volume elements receive an adequate UV-C dose over successive passes. This finding directly supports the Dean-flow reactor design: without the continuous radial transport provided by Dean vortices (De = 491), fluid elements in the central

region would receive negligible UV-C exposure regardless of pass number, rendering the system ineffective for pathogen inactivation in DHM. The integration of a radiation-free central zone with a high-irradiance near-wall annulus, coupled with the strong Dean vortex mixing, constitutes the fundamental mechanism of microbial inactivation efficiency in this system.

3.3. Microbial inactivation

UV-C irradiation inactivates bacteria primarily by absorbing UV-C energy into nucleic acids via pyrimidine and purine bases of DNA, which forms pyrimidine dimers that block replication and transcription (Kurosaki et al., 2003; Rastogi et al., 2010). This light absorption results in chemical reactions (e.g., single- and double-stranded DNA breaks) and the production of photoproducts (e.g., cyclobutene pyrimidine dimers, pyrimidine-pyrimidone) prevents cell replication (Kurosaki et al., 2003; Rastogi et al., 2010). The efficacy of UV-C on microbial reduction in opaque milk depends on delivering effective dose uniformly to overcome the repair and survival mechanism of bacteria (Fiege et al., 2023; Liang et al., 2024; Serio et al., 2026). In this study, the intrinsic UV-C sensitivity of *E. faecium* (ATCC 8459) was first established using a standardized collimated beam apparatus to determine organism-specific D-values and was found to be 4.68 mJ/cm². Moreover, the D-value of *S.* Muenchen corresponds to that of a mutant strain of *Coxiella burnetii* (4.1 mJ/cm^2) in bovine skim milk under UV-C irradiation in a collimated-beam system (Pendyala et al., 2023). The similarity in D-value of *S.* Muenchen and *C. burnetti,* which is known as the most thermally resistant bacteria in dairy processing and hence considered as the target organism for thermal pasteurization validation, suggests that *S.* Muenchen could serve as a surrogate bacterium for *C. burnetti* reduction for various UV-C treatments of DHM (Pendyala et al., 2023). The higher D-value of *E. faecium* (4.68 mJ/cm²) compared with *S.* Muenchen (4.1 mJ/cm²) indicates its relatively greater UV-C tolerance which is consistent with the higher fluences reported for *Enterococcus* spp. than for *Salmonella* spp. in compiled UV-C fluence data (Malayeri et al., 2016). The microbial reduction of both gram-positive and gram-negative bacteria investigated in this study captures a broad range of bacterial structural diversity that may be encountered in DHM. The D-values for *S.* Muenchen and *E. faecium* herein were higher than those observed in previous UV-C studies for most other vegetative bacteria, suggesting that the doses obtained herein for >5-log reductions may be sufficient for most vegetative bacteria in DHM. The D-value of *S.* Muenchen (4.1 mJ/cm²) was used to back-

calculate the delivered REF (mJ/cm²) at each pass in the serpentine Dean-flow system, as presented in Table 2.

Table 2: Calculated reduction-equivalent fluence (REF, mJ/cm^2) in the serpentine Dean-flow UV-C system, delivered in several passes, using inactivation of *S.* Muenchen (ATCC BAA-1674).

Microorganism	No. of passes during Dean-flow UV-C treatment							
S. Muenchen (ATCC BAA-1674))	1st	2nd	3rd	4th	5th	6th	7th	8th
Log inactivation	0.49	1.51	3.64	5.29	5.83	6.83	7.01	7.16
Delivered REF (mJ/cm^2)	2	6.2	14.9	21.7	23.9	28	29	29.4

This REF calculation method takes into consideration the complex optical attenuation of DHM, resulting in an accurate estimation of the effective fluence delivered to the microorganisms (Patras et al., 2021; Pendyala et al., 2022; Singh et al., 2025). As shown in Table 2, the calculated REF values delivered across successive passes increased progressively from 2 mJ/cm² (1st pass) to 29.4 mJ/cm² (8th pass). The corresponding log reductions of *S.* Muenchen were 0.49, 1.5, 3.6, 5.3, 5.8, 6.8, 7 and 7.2 log CFU/mL, respectively, at REF values of 2, 6.2, 14.9, 21.7, 23.9, 28, 29, and 29.4 mJ/cm². For *E. faecium*, the log reductions were 0.42, 1.3, 3.13, 4.6, 5.0, 5.9, 6.0, and 6.2 log CFU/mL at the same REF values (Figure 2).

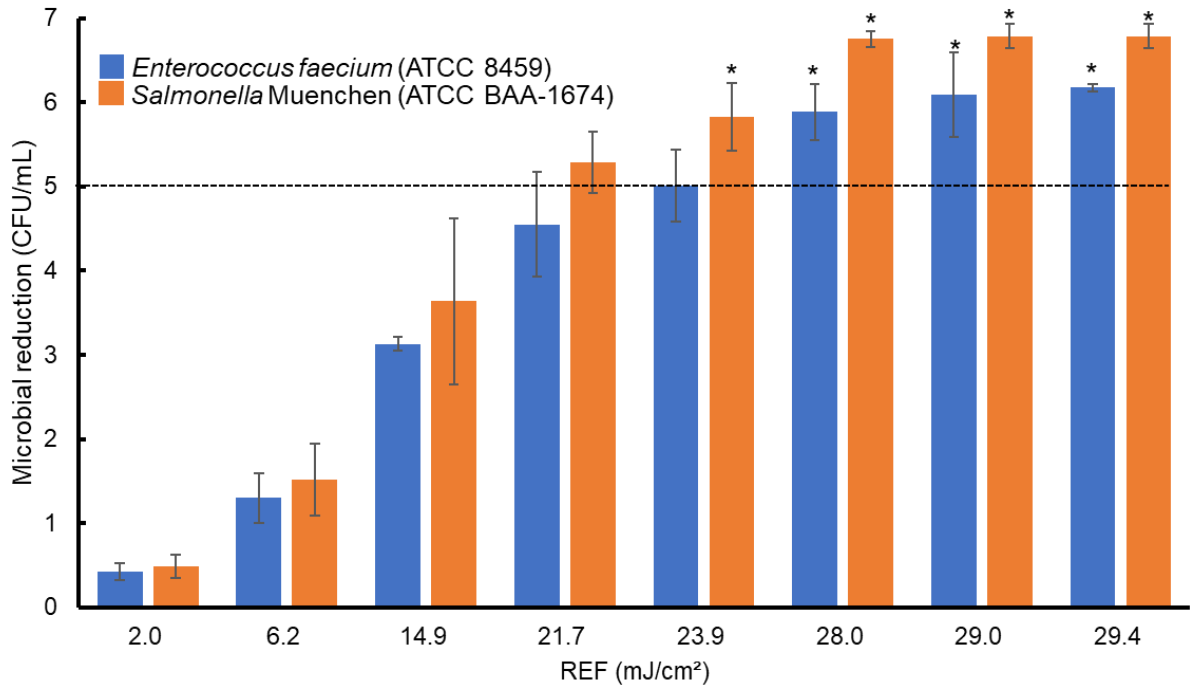

Figure 2: Inactivation data of *E. faecium* (ATCC 8459) and *S.* Muenchen (ATCC BAA-1674) in a lab-scale serpentine Dean-flow UV-C system as a function of varying UV-C dose (2–29.4 mJ/cm^2). Data from 3 independent DHM pools are represented as the mean ± standard deviation. An asterisk (*) indicates that the 95% confidence interval was above the 5-log reduction target. The horizontal dash line indicates a 5-log reduction across the UV-C doses investigated for microbial inactivation.

The microbial inactivation profiles for both *E. faecium* and *S.* Muenchen in DHM, treated through successive passes in the serpentine Dean-flow UV-C system, are presented in Figure 1 as a function of REF. Progressive increases in delivered UV-C fluence showed increased reductions for both organisms, indicating a dose-dependent relationship (Figure 1). A UV-C dose of approximately 28 mJ/cm² (6th pass) provided greater than 5-log reduction for both *S.* Muenchen (6.75 log reduction) and *E. faecium* (5.9 log reduction) with the lower bound of the 95% CI exceeding the 5-log target for both organisms (Figure 2). As we operated the UV-C system under chilled conditions (<10 °C), the observed microbial reduction is due solely to UV-C photoinactivation rather than any synergistic thermal effect. Our results therefore indicate that a UV-C fluence of 28 mJ/cm², applied in a chilled condition, could be an alternative to the current DHM processing standard, HoP, as this REF demonstrated a >5-log reduction in UV-C-resistant gram-positive and gram-negative vegetative bacteria.

3.4 Preservation of bioactive proteins and enzymatic activities

The preservation of bioactive DHM proteins (lactoferrin and IgA) and enzyme activities (BSSL and lysozyme) was measured across all UV-C and HoP-treated samples, and the results are illustrated in Figure 3. In this study, at the optimized UV-C fluence (28 mJ/cm^2) dose, we found significantly ($p < 0.05$) higher preservation of lactoferrin (88.3 ± 7.6%), IgA (89 ± 3.2%), activity of BSSL (74.4 ± 4.7%) and lysozyme (72 ± 5.4%) compared with HoP (14.1 ± 2.4%, 44.1 ± 4.8%, 6.9 ± 4.7% and 9.8 ± 2.5%, respectively) as shown in Figure 3, and continued this trend of preservation even after the highest fluence (29.4 mJ/cm^2) delivered via the serpentine Dean-flow system. These findings are in agreement with previously published works, including our own, finding improved preservation of bioactive milk proteins with UV-C compared with HoP (Christen et al., 2013; Liang et al., 2024).

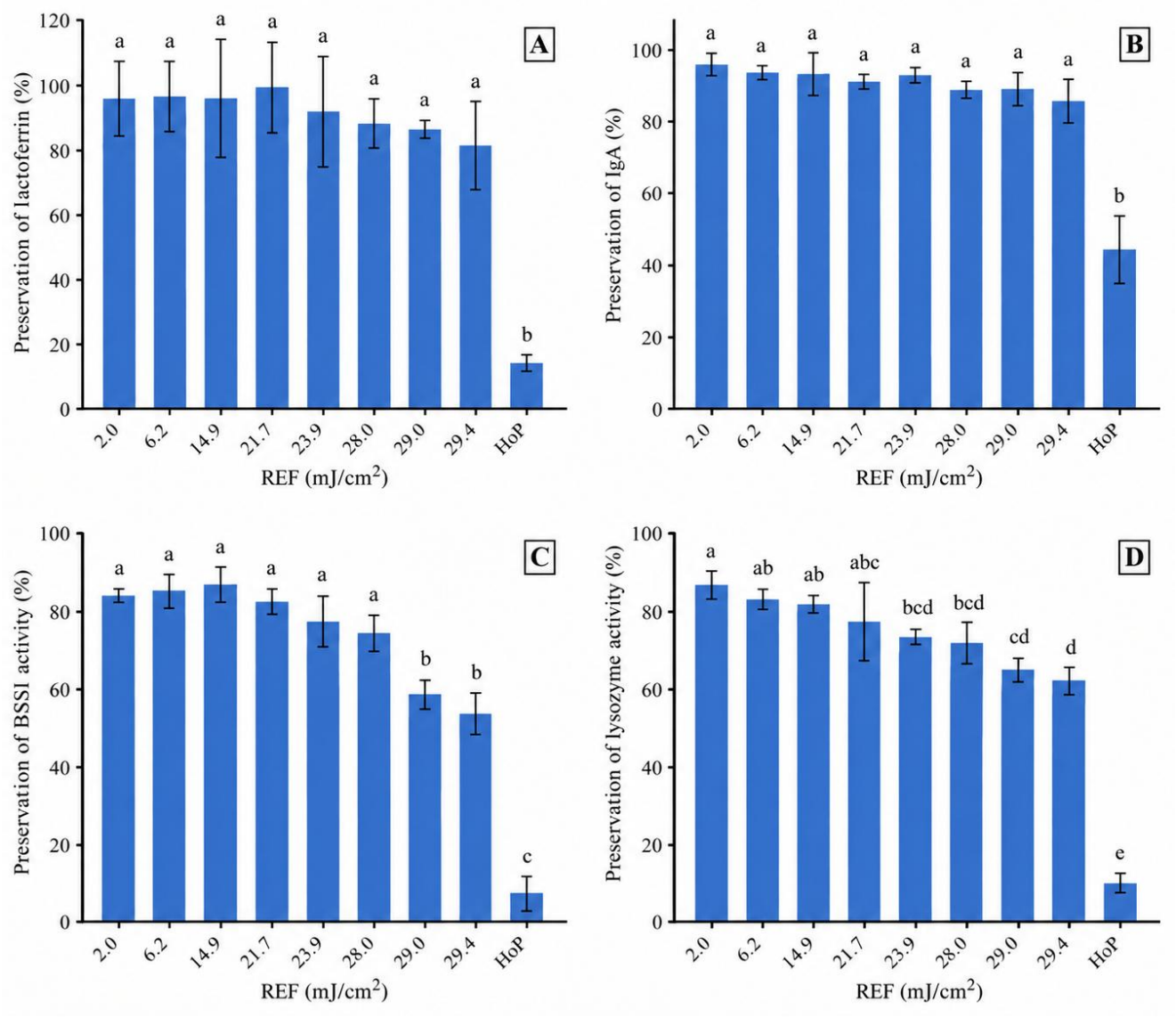

Figure 3: Preservation of the bioactive proteins (%) lactoferrin (A) and immunoglobulin A (IgA, B) and enzymatic activities of bile salt-stimulated lipase (BSSL, C) and lysozyme (D) after exposure to serpentine Dean-flow UV-C processing across varying UV-C doses (2–29.4 mJ/cm^2) compared with HoP-treated DHM. Post-treatment preservation (%) is shown as mean ± standard deviation. Bars not sharing a common letter differ significantly (one-way ANOVA with Tukey's post-hoc testing, $p < 0.05$).

The mechanistic impact of thermal processing on bioactive components and enzyme activities is well documented. Prolonged heating during HoP (62.5 °C for 30 min) induces irreversible unfolding and aggregation of glycoproteins (e.g., lactoferrin and IgA) (Considine et al., 2007). HoP also denatures thermolabile enzymes (e.g., BSSL and lysozyme), as these

enzymes start losing their activities at >45 °C (Kontopodi et al., 2022; Mank et al., 2021). UV-C treatment of DHM in this study was performed in chilled conditions (<10 °C) to avoid the thermal denaturation of bioactive milk proteins and preserve their functionalities. All proteins examined had better preservation with UV-C treatments tested herein than HoP. However, as shown in Figure 3, the preservation of protein and enzyme activities gradually decreased (except for IgA) above the UV-C fluence of 23.9 mJ/cm^2, which could be due to the absorption of photons by proteins (Liang et al., 2024). However, the degree of preservation of bioactive components after UV-C in the published studies varies due to reactor design, dose delivery, dose calculation and efficacy in fluid mixing (Barman, 2025; Singh et al., 2025; Vashisht et al., 2022).

3.5 Preservation of vitamins and extent of lipid oxidation

Further, we measured vitamins A (retinol) and E (α-tocopherol) in HoP- and UV-C-treated samples at the 28 mJ/cm^2 fluence optimized for >5-log reduction in both bacteria investigated herein. The optimized fluence (28 mJ/cm^2) resulted in higher preservation of vitamin A (60.4 ± 4.7%) compared with HoP (48.6 ± 4.8%) ($p < 0.05$). Similar preservation levels were observed for vitamin E between UV-C-treated (61.4 ± 9.8%) and HoP-treated (61.5 ± 9.8%) DHM samples, consistent with our previously published work (Liang et al., 2024). The degradation of Vitamin A (retinol) after HoP could result from heat-mediated isomerization of retinoid chromophore and oxidative degradation (Lešková et al., 2006).

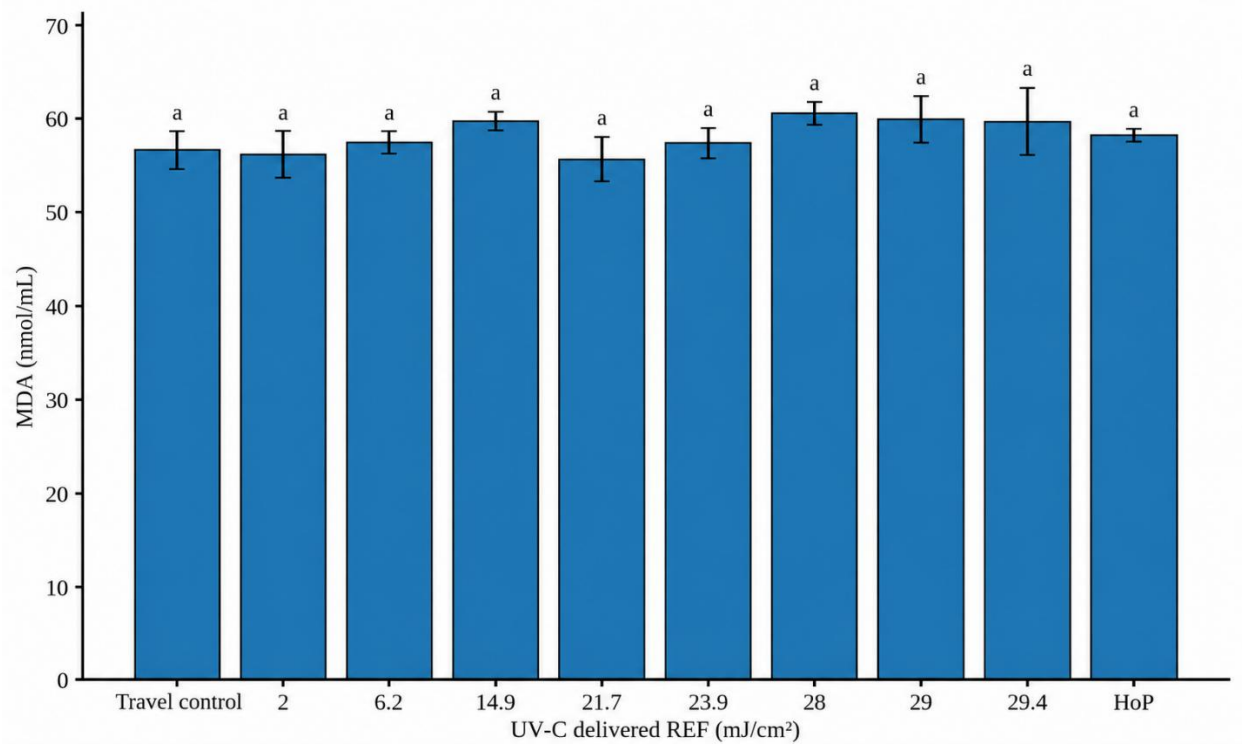

Figure 4: Total MDA concentration (nmol/mL) in DHM after exposure to serpentine Dean-flow UV-C processing across varying UV-C doses (2–29.4 mJ/cm^2) compared with HoP-treated and untreated (travel control) DHM. MDA concentration is shown as mean ± standard deviation. Bars sharing a common letter are not significantly different (one-way ANOVA with Tukey's post-hoc testing, $p < 0.05$).

The concentration of the lipid oxidation product MDA was measured across all untreated, UV-C- and HoP-treated samples, and the results are shown in Figure 4. MDA values were 56.59 ± 2.00 nmol/mL for untreated DHM, 58.19 ± 0.68 nmol/mL after HoP and ranged from 56.12 ± 2.52 to 59.68 ± 3.59 nmol/mL for UV-C treatments (Figure 4). Our results suggest that under the processing conditions tested herein, Dean-flow UV-C treatment did not promote detectable MDA accumulation and thus did not stimulate secondary lipid oxidation in DHM ($p > 0.05$). The lack of changes in MDA concentration in DHM before and after UV-C and HoP treatments align with previous work (Liang et al., 2024; Silvestre et al., 2008). However, another study reported a 36% increase in MDA concentration in DHM after UV-C (Martysiak-Żurowska et al., 2017). Differences in MDA concentration between that study and the current results may be due to differences in UV-C reactor configuration, dose calculations, hydrodynamic mixing and temperature control. The absence of significant MDA formation at the delivered UV-C doses of

2.0–29.4 mJ/cm² (Figure 4) indicates that the process could achieve microbial safety without a measurable increase in secondary lipid oxidation in DHM.

4. Conclusion

Overall, our optimized UV-C fluence (28 mJ/cm^2) achieved >5-log reduction in vegetative bacteria in DHM and better preserved bioactive proteins and enzymatic activities compared with conventional HoP, providing evidence to consider the adoption of serpentine Dean-flow UV-C for donor human milk banks. For vitamins, we found that UV-C led to similar or better preservation of A and E and did not increase MDA, a marker of secondary lipid oxidation. Though this work was carried out using multiple passes in a lab-scale system, which would not be ideal for milk bank conditions, we have already scaled up this UV-C system, and a production-scale continuous serpentine Dean-flow system is now commercially available (FloUV, TN, USA). Future work should examine the effects of this UV-C processing system and fluence on additional vegetative bacteria and spores, additional bioactive components and individual lipids. Future work should also examine the effects of this UV-C-treated milk in animal models and infants to determine the extent to which the improved preservation of bioactive proteins results in improved biological outcomes such as growth and gut health. Such investigations are necessary to move this technology toward use in donor human milk banks and in clinical settings.

Data availability

The data supporting the findings of this study are presented in the main text, figures, tables and Supplementary Information. The underlying experimental datasets generated and analyzed during this study are available from the corresponding author upon reasonable request.

Funding

This study was funded by the National Institutes of Health (grant no. 5R01HD106140).

Acknowledgements

The authors thank Scott William Leonard at the Linus Pauling Institute at Oregon State University for the analyses of vitamins A and E. The Northwest Mother's Milk Bank, Tigard, OR, provided all donor milk used in this study.

Author contributions

M.A.W. contributed to study conceptualization, experimental design, sample preparation, investigation, biochemical analyses, data analysis, visualization and writing the original

manuscript draft. J.B. and N.T. contributed to experimental investigation, optical characterization, UV-C processing, microbial inactivation studies, data analysis, review and editing. H.M. contributed to microbial inoculation and enumeration, review and editing. B.B. contributed to review and editing. R.L.L. contributed to MDA analysis, data interpretation, review and editing. B.P. contributed to computational fluid dynamics simulations, radiation modeling, formal analysis, and visualization. A.P. contributed to optical characterization, UV-C processing methodology, experimental design, manuscript review and editing. J.W.-C. contributed to microbiological study design, data interpretation, manuscript review and editing. D.C.D. contributed to study conceptualization, funding acquisition, project administration, supervision, data interpretation and manuscript review and editing. All authors reviewed and approved the final version of the manuscript.

Competing interests

The authors declare no competing interests.

References

Akwu, A. S., Patras, A., Pendyala, B., Kurup, A. H., Chen, F., Boushra, M., . . . Vergne, M. J. (2023). Effect of germicidal short wavelength ultraviolet light on the polyphenols, vitamins, and microbial inactivation in a highly opaque apple juice. *Journal of Food Safety, 43*(3), e13037.

Ballard, O., & Morrow, A. L. (2013). Human milk composition: nutrients and bioactive factors. *Pediatric Clinics, 60*(1), 49–74.

Barman, B. (2025). Batch vs. continuous ultraviolet-C (UV-C) processing of bovine milk: a comparison of the effects of≥ 5-log reduction UV-C dosage on the bioactive proteins of bovine milk.

Barman, B., Sykora, R., Mohamed, H., Paviani, B., Singh, S., Waite-Cusic, J., . . . Dallas, D. C. (2026). UV-C processing of bovine milk: Dosage requirements for 5-log bacterial reductions and impact on the bioactive proteins. *Food Research International,* , 119023.

Bertino, E., Giribaldi, M., Baro, C., Giancotti, V., Pazzi, M., Peila, C., . . . Cavallarin, L. (2013). Effect of prolonged refrigeration on the lipid profile, lipase activity, and oxidative status of human milk. *Journal of Pediatric Gastroenterology and Nutrition, 56*(4), 390–396.

Bolton, J. R., & Linden, K. G. (2003). Standardization of methods for fluence (UV dose) determination in bench-scale UV experiments. *Journal of Environmental Engineering, 129*(3), 209–215.

Cao, X., Ren, Y., Lu, Q., Wang, K., Wu, Y., Wang, Y., . . . Chen, Z. (2023). Lactoferrin: A glycoprotein that plays an active role in human health. *Frontiers in Nutrition, 9*, 1018336.

Christen, L., Lai, C. T., Hartmann, B., Hartmann, P. E., & Geddes, D. T. (2013). The effect of UV-C pasteurization on bacteriostatic properties and immunological proteins of donor human milk. *PLOS One, 8*(12), e85867.

Collins, A., Weitkamp, J., & Wynn, J. L. (2018). Why are preterm newborns at increased risk of infection? *Archives of Disease in Childhood-Fetal and Neonatal Edition, 103*(4), F391–F394.

Conboy-Stephenson, R., Ross, R. P., Kelly, A. L., & Stanton, C. (2024). Donor human milk: the influence of processing technologies on its nutritional and microbial composition. *Frontiers in Nutrition, 11*, 1468886.

Considine, T., Patel, H. A., Anema, S. G., Singh, H., & Creamer, L. K. (2007). Interactions of milk proteins during heat and high hydrostatic pressure treatments—A review. *Innovative Food Science & Emerging Technologies, 8*(1), 1–23.

Demers-Mathieu, V., Qu, Y., Underwood, M. A., Borghese, R., & Dallas, D. C. (2018). Premature infants have lower gastric digestion capacity for human milk proteins than term infants. *Journal of Pediatric Gastroenterology and Nutrition, 66*(5), 816–821.

Fenaille, F., Mottier, P., Turesky, R. J., Ali, S., & Guy, P. A. (2001). Comparison of analytical techniques to quantify malondialdehyde in milk powders. *Journal of Chromatography A, 921*(2), 237–245.

Ferraboschi, P., Ciceri, S., & Grisenti, P. (2021). Applications of lysozyme, an innate immune defense factor, as an alternative antibiotic. *Antibiotics, 10*(12), 1534.

Fiege, J. L., Woll, B., Hebig, S., Dabrowski, A., Graf, V., Walz, E., . . . Stahl, M. (2023). Observation of a temperature dependent anomaly in the UV translucency of milk useful for UV-C preservation techniques. *Scientific Reports, 13*(1), 21937–y. doi:10.1038/s41598-023-49124-y

Gunter-Ward, D. M., Patras, A., S. Bhullar, M., Kilonzo-Nthenge, A., Pokharel, B., & Sasges, M. (2018). Efficacy of ultraviolet (UV-C) light in reducing foodborne pathogens and model viruses in skim milk. *Journal of Food Processing and Preservation, 42*(2), e13485.

He, X., McClorry, S., Hernell, O., Lonnerdal, B., & Slupsky, C. M. (2020). Digestion of human milk fat in healthy infants. *Nutrition Research (New York, N.Y.), 83*, 15–29. doi:10.1016/j.nutres.2020.08.002

Kamao, M., Tsugawa, N., Suhara, Y., Wada, A., Mori, T., Murata, K., . . . Tanaka, K. (2007). Quantification of fat-soluble vitamins in human breast milk by liquid chromatography–tandem mass spectrometry. *Journal of Chromatography B, 859*(2), 192–200.

Kaushik, S., Wander, R., Leonard, S., German, B., & Traber, M. G. (2001). Removal of fat from cow's milk decreases the vitamin E contents of the resulting dairy products. *Lipids, 36*(1), 73–78.

Kim, B. J., Ryan, M. B., & Dallas, D. C. (2025). Ultraviolet-C Treatment Better Preserves the Proteomic Profile of Donor Human Milk than Holder Pasteurization. *Journal of Agricultural and Food Chemistry, 73*(39), 25076.

Koh, J., Victor, A. F., Howell, M. L., Yeo, J. G., Qu, Y., Selover, B., . . . Dallas, D. C. (2020). Bile salt-stimulated lipase activity in donor breast milk influenced by pasteurization techniques. *Frontiers in Nutrition, 7*, 552362.

Kontopodi, E., Boeren, S., Stahl, B., van Goudoever, J. B., van Elburg, R. M., & Hettinga, K. (2022). High-temperature short-time preserves human milk's bioactive proteins and their function better than pasteurization techniques with long processing times. *Frontiers in Pediatrics, 9*, 798609.

Koutchma, T. (2018). Status of international regulations for ultraviolet treatment of foods. *IUVA News, 20*(2), 13–16.

Kurosaki, Y., Abe, H., Morioka, H., Hirayama, J., Ikebuchi, K., Kamo, N., . . . Ikeda, H. (2003). Pyrimidine Dimer Formation and Oxidative Damage in M13 Bacteriophage Inactivation by Ultraviolet C Irradiation¶. *Photochemistry and Photobiology, 78*(4), 349–354.

Lešková, E., Kubíková, J., Kováčiková, E., Košická, M., Porubská, J., & Holčíková, K. (2006). Vitamin losses: Retention during heat treatment and continual changes expressed by mathematical models. *Journal of Food Composition and Analysis, 19*(4), 252–276.

Liang, N., Mohamed, H., Pung, R. F., Waite-Cusic, J., & Dallas, D. C. (2024). Optimized ultraviolet-C processing inactivates pathogenic and spoilage-associated bacteria while preserving bioactive proteins, vitamins and lipids in human milk. *Journal of Agricultural and Food Chemistry, 72*(21), 12198.

Malayeri, A. H., Mohseni, M., Cairns, B., Bolton, J. R., Chevrefils, G., Caron, E., . . . Linden, K. G. (2016). Fluence (UV dose) required to achieve incremental log inactivation of bacteria, protozoa, viruses and algae. *IUVA News, 18*(3), 4–6.

Mank, E., Kontopodi, E., Heijboer, A. C., Van Elburg, R. M., Hettinga, K., van Goudoever, J. B., & van Toledo, L. (2021). Thermoultrasonication, ultraviolet-C irradiation, and high-pressure processing: Novel techniques to preserve insulin in donor human milk. *Clinical Nutrition, 40*(11), 5655–5658.

Martysiak-Żurowska, D., Puta, M., Kotarska, J., Cybula, K., Malinowska-Pańczyk, E., & Kołodziejska, I. (2017). The effect of UV-C irradiation on lipids and selected biologically active compounds in human milk. *International Dairy Journal, 66*, 42–48.

Matak, K. E., Churey, J. J., Worobo, R. W., Sumner, S. S., Hovingh, E., Hackney, C. R., & Pierson, M. D. (2005). Efficacy of UV light for the reduction of Listeria monocytogenes in goat's milk. *Journal of Food Protection, 68*(10), 2212–2216.

Moro, G. E., Billeaud, C., Rachel, B., Calvo, J., Cavallarin, L., Christen, L., . . . Wesolowska, A. (2019). Processing of donor human milk: update and recommendations from the European Milk Bank Association (EMBA). *Frontiers in Pediatrics, 7*, 49.

Müller, A., Stahl, M. R., Graef, V., Franz, C. M., & Huch, M. (2011). UV-C treatment of juices to inactivate microorganisms using Dean vortex technology. *Journal of Food Engineering, 107*(2), 268–275.

Patras, A., Bhullar, M. S., Pendyala, B., & Crapulli, F. (2021). Ultraviolet treatment of opaque liquid foods: from theory to practice.

Peila, C., Emmerik, N. E., Giribaldi, M., Stahl, B., Ruitenberg, J. E., Van Elburg, R. M., . . . Cavallarin, L. (2017). Human milk processing: a systematic review of innovative

techniques to ensure the safety and quality of donor milk. *Journal of Pediatric Gastroenterology and Nutrition, 64*(3), 353–361.

Pendyala, B., Patras, A., Gopisetty, V. V. S., & Sasges, M. (2021). UV-C inactivation of microorganisms in a highly opaque model fluid using a pilot scale ultra-thin film annular reactor: Validation of delivered dose. *Journal of Food Engineering, 294*, 110403.

Pendyala, B., Patras, A., Gopisetty, V. V. S., Vashisht, P., & Ravi, R. (2022). Inactivation of B. cereus spores in whole milk and almond milk by serpentine path coiled tube UV-C system: Numerical simulation of flow field, lipid peroxidation and volatiles analysis. *Food Research International, 160*, 111652.

Pendyala, B., Patras, A., Ravi, R., Gopisetty, V. V. S., & Sasges, M. (2020). Evaluation of UV-C irradiation treatments on microbial safety, ascorbic acid, and volatile aromatics content of watermelon beverage. *Food and Bioprocess Technology, 13*(1), 101–111.

Pendyala, B., Vashisht, P., Chen, F., Sanchez, S. E., Comstock, B., Omsland, A., & Patras, A. (2023). Evaluating the UV-C sensitivity of Coxiella burnetii in skim milk using a bench-scale collimated beam system and comparative thermal sensitivity study by high-temperature short-time pasteurization. *Frontiers in Food Science and Technology, 3*, 1251069.

Prahl, S. (1999). Optical property measurements using the inverse adding-doubling program. *Oregon Medical Laser Center, St.Vincent Hospital, 9205*, 1–53.

Quigley, M., Embleton, N. D., & McGuire, W. (2019). Formula versus donor breast milk for feeding preterm or low birth weight infants. *Cochrane Database of Systematic Reviews,* (7)

Rastogi, R. P., Richa, n., Kumar, A., Tyagi, M. B., & Sinha, R. P. (2010). Molecular mechanisms of ultraviolet radiation-induced DNA damage and repair. *Journal of Nucleic Acids, 2010*(1), 592980.

Serio, J., Santos, C., Martins, M. E., Marques, A. P., Feliciano, C., Serrano, M., . . . Pereira, V. J. (2026). UV-C LED wavelength effects on inactivation kinetics, DNA damage and membrane integrity in drinking water indicator bacteria. *Scientific Reports, 16*(1), 15919. doi: 10.1038/s41598–8. doi:10.1038/s41598-026-44556-8

Silvestre, D., Miranda, M., Muriach, M., Almansa, I., Jareño, E., & Romero, F. J. (2008). Antioxidant capacity of human milk: effect of thermal conditions for the pasteurization. *Acta Paediatrica, 97*(8), 1070–1074.

Singh, A., Sharma, A., Pendyala, B., Balamurugan, S., & Patras, A. (2025). Efficacy of a continuous dean flow UV-C system in almond milk treatment using computational fluid dynamics and biodosimetry. *Food and Bioprocess Technology, 18*(3), 2697–2708.

Tanner, S. M., Berryhill, T. F., Ellenburg, J. L., Jilling, T., Cleveland, D. S., Lorenz, R. G., & Martin, C. A. (2015). Pathogenesis of necrotizing enterocolitis: modeling the innate immune response. *The American Journal of Pathology, 185*(1), 4–16.

Vashisht, P., Pendyala, B., Gopisetty, V. V. S., & Patras, A. (2021). Modeling and validation of delivered fluence of a continuous Dean flow pilot scale UV system: monitoring fluence by biodosimetry approach. *Food Research International, 148*, 110625.

Vashisht, P., Pendyala, B., Patras, A., Gopisetty, V. V. S., & Ravi, R. (2022). Design and efficiency evaluation of a mid-size serpentine Dean flow UV-C system for the processing of whole milk using computational fluid dynamics and biodosimetry. *Journal of Food Engineering, 335*, 111168.

Walker, A. (2010). Breast milk as the gold standard for protective nutrients. *Journal of Pediatrics, 156*(2), S3–S7.

Supplementary Files

This is a list of supplementary files associated with this preprint. Click to download.

- Supplementaryfile.pdf